Eur. Phys. J. B **41**, 3–9 (2004)
DOI: 10.1140/epjb/e2004-00287-5

THE EUROPEAN PHYSICAL JOURNAL B

Influence of growth mode on stoichiometry in epitaxial calcium ruthenate thin films

U. Scotti di Uccio[1,2,a], F. Bevilacqua[2,b], G.G. Condorelli[3], G. Mascolo[1], F. Ricci[4,c], and F. Miletto Granozio[2]

[1] Di.M.S.A.T., Università di Cassino, via di Biasio 43, 03043 Cassino, Italy
[2] Coherentia-INFM, P.le Tecchio 80, 80125 Napoli, Italy
[3] Dip. Scienze Chimiche, Università di Catania, Catania, Italy
[4] Dip. Scienze Fisiche, Università Federico II di Napoli, e Coherentia-INFM, P.le Tecchio 80, 80125 Napoli, Italy

Received 29 May 2003 / Received in final form 13 April 2004
Published online 30 September 2004 –

Abstract. Clear evidence about the influence of growth orientation on the stoichiometry of sputtered oxide thin films is reported and discussed. The growth of stoichiometric and of non-stoichiometric films is respectively obtained, from the same $CaRuO_3$ target, on the surface of (110) and (100) perovskite substrates. Such phenomenon has been systematically investigated by deposition of pairs of samples in the same deposition run. Our data show that in samples deposited on (100) perovskites, Ca excess leads to the formation of a single Ca-rich phase with stoichiometry $Ca_{1+x}Ru_{1-x}O_3$, resulting in a dramatic effect on transport properties. Structural characterization based on X-ray diffraction proves that the orthorhombic structure is preserved in a wide stoichiometry range. The striking evidence that substrate orientation influences film stoichiometry is discussed in terms of growth kinetics and chemical properties of sputtered species.

PACS. 68.55.-a Thin film structure and morphology

1 Introduction

High quality epitaxial films of simple perovskitic materials (ABO_3) are usually grown resorting to different physical vapor deposition techniques, including a number of different sputtering configurations. Roughly, the film growth proceeds through three different steps. As a first step, the impinging species ejected from the target are captured by the substrate surface, where they remain as mobile adatoms. As a second step, the formation of the smallest, stable grains (nuclei) of the film phase occurs. Finally, supercritical nuclei grow at a rate that is essentially limited by kinetics, and is related to the geometry of the growing front (2D or 3D growth, etc.). All these processes have been thoroughly investigated since decades both from the experimental and the theoretical point of view [1], but most of this work is related to films made up of a single atomic species. Interest in transition metal oxides, as high temperature superconductors, has more recently attracted the attention of researchers on the growth of complex compounds in reactive conditions. However, several relevant aspects of such growth process still remain partially unknown.

In this paper we focus our attention on the effect of the growth surface crystallographic orientation on the stoichiometry of epitaxial $CaRuO_3$ (CRO) films deposited by sputtering from a single target. $CaRuO_3$ is a bad metal, with room temperature resistivity $\rho_{300} \sim 270$ $\mu\Omega$ cm. It is characterized by a very complex electronic structure, largely determined by the 4d Ru orbitals, and by their overlapping with $2p$ O orbitals. At difference to $SrRuO_3$, that is a robust ferromagnet with Curie temperature $T_C = 165$ K [2], CRO is not ferromagnetic, and the nature of its magnetic ordering is still under investigation [3]. A dramatic effect of doping on electric transport has been reported [8], as also confirmed by the data presented in this work. It is suggested that CRO is a strongly correlated material on the verge of a Mott metal-insulator transition.

One of the main experimental results emerging from this work, is the clear signature of an influence of crystallographic orientation on the stoichiometry of the deposited films, and hence on their transport properties. Indeed, this might seem quite surprising, since such an evidence has probably never emerged before on this class of compounds. Deviations from stoichiometry in sputtered films are generally related to less subtle mechanisms: e.g., selective sputtering at target surface, backsputtering on films surface, aging of target, difference in angular spreads for the different atomic species. However, if growth takes place

[a] e-mail: scotti@na.infn.it
[b] *Present address*: STMicroelectronics, Arzano, Italy
[c] *Present address*: Pirelli Labs, Italy

in incomplete condensation conditions [1] the lifetime τ_a of adatoms on the growth surface can affect stoichiometry. In turn, τ_a is highly sensitive to surface properties that may well be anisotropic.

Reported data have been collected during our work on CRO films grown on $SrTiO_3$, $LaAlO_3$, and $NdGaO_3$ substrates with exact (110) and (100) termination. We routinely obtain high quality films on (110) perovskitic substrates [4]. Under identical deposition conditions, and even in the same deposition run, non-stoichiometric films are instead obtained on (100) perovskites.

Stoichiometry deviations have been previously reported by Rao et al. [5] on CRO samples deposited by off-axis sputtering on (100) $SrTiO_3$ and (100) $LaAlO_3$. The authors propose that Ca-rich samples are obtained when the CRO film is grown under tensile strain, as for deposition on $SrTiO_3$, while stoichiometric samples are obtained when samples are grown on $LaAlO_3$, that is, in compressive strain. This is attributed to the larger size of the Ca ion, and consequently to the larger lattice parameter of the substituted samples, leading to stress relief for samples in tensile strain. The growth of metallic films is instead reported on (100) $LaAlO_3$ single crystals, where the compressive strain induced by the substrate is believed to disfavor Ca substitution. The extended study reported in this work, confirms that samples with poor conducting properties are obtained in specific deposition conditions, and that such samples are Ca rich, and yet single phase. Nevertheless, our data obtained from film deposition on six different kinds of substrate surfaces suggest a different driving mechanism triggering the growth of non-stoichiometric films.

Recognizing and interpreting the mechanism leading to the growth of Ca rich CRO films, and studying their properties, is important for several reasons. First, reported data suggest some intriguing relation between growth mode and film stoichiometry, that will be addressed in detail. Second, Ca excess in the films results, rather than in the formation of precipitates, in the growth of a new Ca rich solid solution, whose properties are still unknown, covering a wide range of different stoichiometries and transport properties. Finally, studies on presumably Ca rich CRO films with relatively poor or inhomogeneous conducting properties have been recently reported in literature [6,7]. It is important to clearly distinguish the physical properties that are intrinsic to stoichiometric $CaRuO_3$, from those of Ca-rich samples, since electronic properties of $CaRuO_3$ are dramatically affected by even small deviations from the 1:1:3 stoichiometry [8] and by disorder [9].

2 Experimental results

The CRO thin films were deposited by on-axis magnetron sputtering from a CRO target with 1:1:3 nominal stoichiometry. The process gas pressures P_{Ar} and P_{O2} were kept equal, in the range 1.3–6.6 Pa. Substrate temperature was varied in the range 650–750 °C, and target-to-substrate distance was varied in the range 13–40 mm. (100) and (110) oriented $SrTiO_3$ (STO), $LaAlO_3$ (LAO), $NdGaO_3$ (NGO) single crystals were employed as substrates.

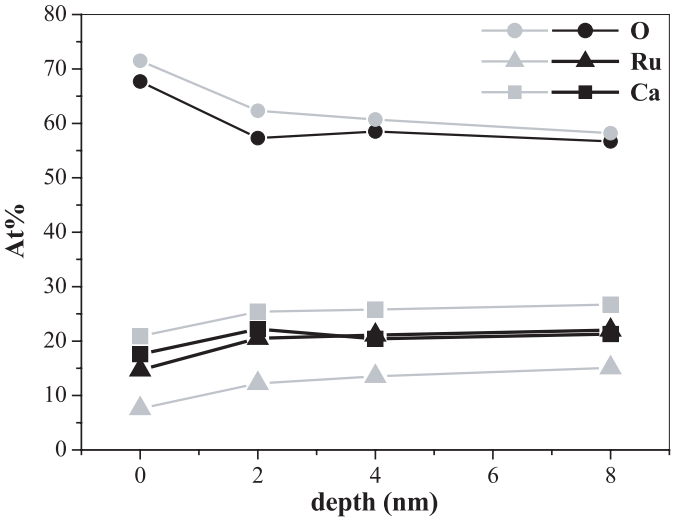

Fig. 1. XPS depth profiles of the Ru^{4+} 3*d*, Ca^{2+} 2*p*, O^{2-} 1*s* emissions at 281.1 eV, 345.0 eV, 528.6 eV, respectively, for the "A" sample (CRO on (110) STO; black symbols) and the "B" sample (CRO on (100) STO; gray symbols).

In most part of the present work, we will not address the orthorhombic distortion of $CaRuO_3$ and $NdGaO_3$ lattices. We will therefore mostly refer, when reporting the Miller indices, to pseudocubic (p.c.) lattices. Only few details about the presence of multiple domains in $CaRuO_3$ will be discussed, while a more a detailed study was reported elsewhere [4].

Structure, transport, morphology and chemistry of deposited samples were respectively probed by X-ray diffraction (XRD), resistivity measurements, X-ray photoemission spectroscopy (XPS), scanning electron microscopy (SEM) and energy dispersive X-ray (EDX) spectroscopy. XRD and XPS setups have been described elsewhere [10,11].

In Figure 1, the XPS depth profile of two different samples, respectively grown in the same deposition run on (110) and (100) STO single substrates, is reported. Within a few nm from the surface, the Ca:Ru:O ratio of sample 1, grown on (110) STO, approaches the 1:1:3 value. The case of sample 2, grown on (100) STO, is different; a ∼30% Ca excess, and ∼30% Ru depletion with respect to 1:1:3 stoichiometry are observed, suggesting a partial substitution of Ca in the Ru sites. This idea will be further discussed in the framework of the whole experimental evidence. In the following, we will employ the notation $Ca_{1+x}Ru_{1-x}O_y$ to denote the stoichiometry of our samples. The value of x (Ca excess) has been also measured by EDX spectroscopy on a wide number of samples. We always found low values of x (at worst, $x = 0.06$) for all the samples grown on (110) STO, (110) LAO and $(100)_{p.c.}$ NGO, denoted in the following as "A" samples. Larger x is systematically obtained for samples grown on (100) STO, (100) LAO and $(110)_{p.c.}$ NGO ("B" samples).

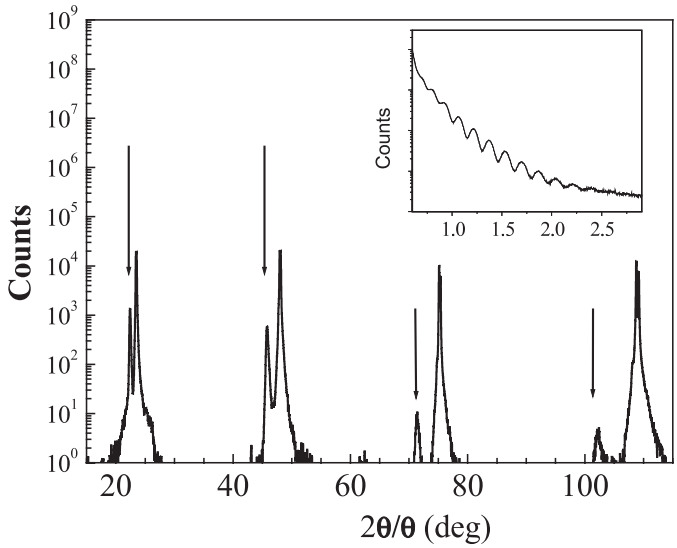

Fig. 2. Log-scale θ-2θ scan of a CRO film deposited on (100) LAO. The arrows indicate the $(\ell 00)_{\text{p.c.}}$ reflections of CRO; the other peaks are the $(\ell 00)$ reflections of LAO. The inset shows the low angle reflectivity of the same sample.

The structural characterization was performed resorting to symmetric θ-2θ scans, ω- and ϕ-scans, and reciprocal space mapping (RSM) of symmetric and non-symmetric reflections. We determined the unit cell symmetry and the orientation of the principal axes with respect to substrate axes. Moreover, we evaluated the length of the lattice parameters and the relative angles, including strain effects, in order to calculate the unit cell volume. The analysis was performed on different films than those reported in Figure 1, since the depth profile required ion milling on a wide portion of sample.

Data regarding "A" films have already been published [4], and will not be presented here. Therefore, we focus our attention on "B" samples. In Figure 2 we report a typical scan of a CRO film grown on (100) $LaAlO_3$. The inset shows the reflectivity at low angles. The interference pattern is very clear, thus demonstrating the high surface quality and smoothness of the sample. The film thickness is determined by reflectivity plots ($t = 49.6 \pm 0.6$ nm in this case shown in the inset), allowing us to calibrate the sputtering rate (0.05 nm s^{-1} under typical sputtering conditions). The θ-2θ scans alone are generally of scarce utility, also due to possible overlapping of $(\ell 00)$ reflections of sample and substrate. More information is achieved by mapping of reciprocal space around the regions of the $(400)_{\text{p.c.}}$, $(330)_{\text{p.c.}}$ and $(401)_{\text{p.c.}}$ CRO reflections. Two such maps are shown in Figure 3 for a sample deposited on (100) STO (a) and on (100) LAO (b). The refinement of the reflections attributed to CRO in the quoted maps allowed us to determine epitaxial relations, strain and lattice spacing of CRO.

Within the simplified scheme of pseudocubic (p.c.) cells, one general result of our complete XRD investigation is that CRO grows "cube on cube" on the considered substrates. In other terms, "B" samples are $(100)_{\text{p.c.}}$ oriented, while "A" samples are $(110)_{\text{p.c.}}$ oriented [4].

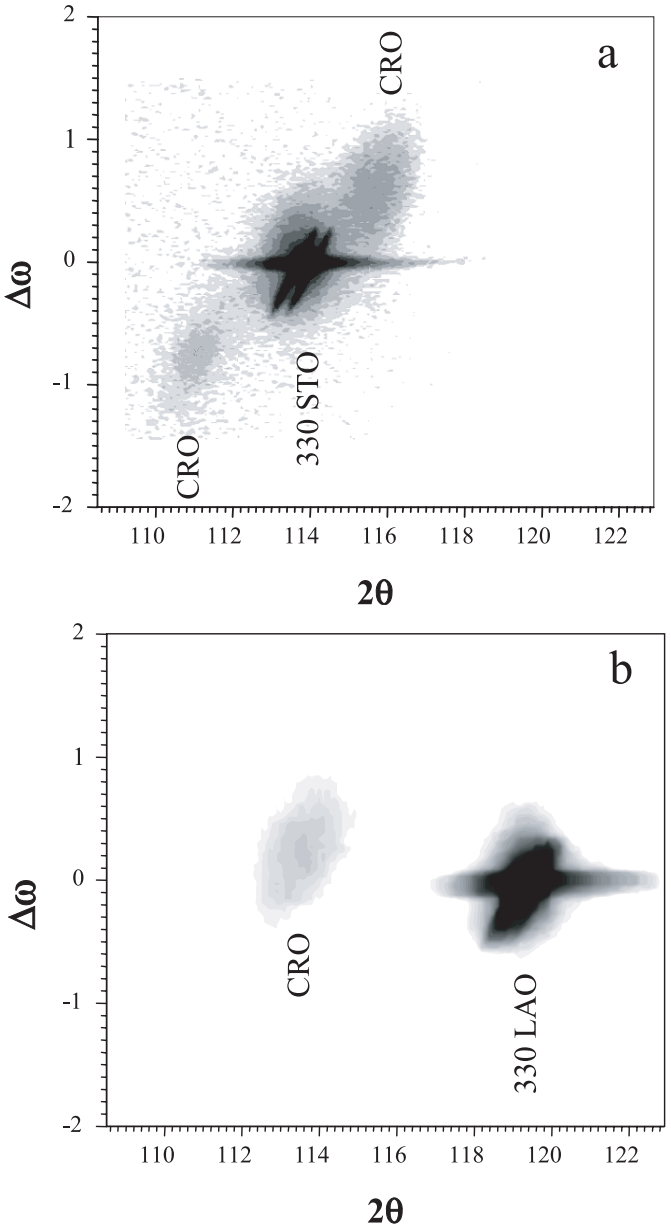

Fig. 3. RSM around the (330) substrate reflection for films deposited on (100) STO (a) and on (100) LAO (b). The peak attributed to CRO is split in (a) due to the orthorhombic deformation; the reflections are indexed as $(600)_{\text{o.r.}}$ and $(060)_{\text{o.r.}}$ in the orthorhombic base [4]. Sample (b) is instead tetragonal, and the reflection is indexed as $(330)_{\text{pc}}$.

Our measurements however reveal a clear difference between "A" and "B" films. While the "A" samples always exhibit cell volumes close to the bulk, the cell volumes of "B" samples spread over a wide range, from the value of the bulk CRO up to 0.063 nm^3 (for the pseudocubic cell), implicating up to ≈10% volume increase. Another striking difference is the following: while "A" samples are strained and well matched to the substrates [4], "B" samples are not matched, still presenting some deviation from the cubic structure. For example, the lattice parameters of the sample of Figure 3a, in orthorhombic notation, are

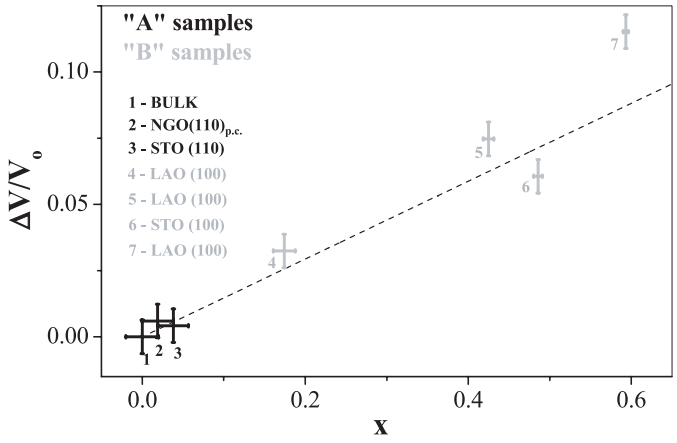

Fig. 4. Percent volume variation vs. Ca excess x . The dotted line is the plot of equation (1). Black symbols denote "A" samples, gray symbols "B" samples.

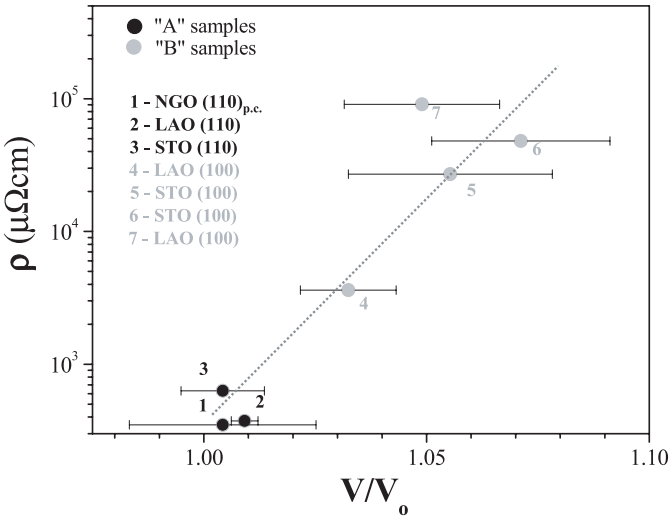

Fig. 5. Room temperature resistivity ρ_{300} vs. cell volume for CRO film grown on different substrates. V_o denotes the volume of bulk stoichiometric CRO. Black symbols denote "A" samples, gray symbols "B" samples. The dotted line is just a guide to the eye.

respectively $a = 0.547 \pm 0.002$ nm, $b = 0.560 \pm 0.002$ nm, $c = 0.779 \pm 0.002$ nm, that is, each one is 1–2% larger with respect to bulk value. The lattice parameters of the sample in Figure 3b, expressed this time in pseudocubic notation, are $a = 0.389 \pm 0.002$ nm, $b = 0.389 \pm 0.002$ nm, $c = 0.393 \pm 0.002$ nm. Also in this case the expansion of the cell affects all the crystal directions, and the stress due to substrate does not play a major role: in the reported cases, the larger in-plane spacing is obtained on $LaAlO_3$, having a smaller lattice parameter than $SrTiO_3$.

While our previous investigation proved that stoichiometric $(110)_{\text{p.c.}}$ CRO films deposited on perovskites are orthorhombic [4], this does not always apply to $(100)_{\text{p.c.}}$. In fact, the orthorhombic distortion is only preserved for moderate values of Ca excess, as demonstrated by reciprocal space mapping in the region of the (330) STO peak. In the orthorhombic structure, the $(330)_{\text{pc}}$ CRO reflection is split in two different peaks. In Figure 3a, the two peaks are found near the (330) STO reflection. In the correct orthorhombic (o.r.) notation, they are identified as $(600)_{\text{o.r.}}$ and $(060)_{\text{o.r.}}$ CRO. On the other hand, the reciprocal space mapping of a sample with $x \approx 0.3$ (Fig. 3b) only shows one CRO reflection. This means that the a and b orthorhombic axes have approached each other, and the structure has turned to tetragonal. On the base of our data, we also speculate that the tetragonal lattice parameters found on highly substituted samples are to be attributed to a strained cubic structure.

The excess Ca detected by XPS and EDX analyses turned out to be closely related to the relative cell volume increment $\frac{\Delta V}{V_o}$ (V_o being the CRO single crystal volume). $\frac{\Delta V}{V_o}$ is plotted vs. x for a group of "A" and "B" samples in Figure 4. The linear relation strongly suggests that the excess Ca is included in the structure, and that the greater dimension of the Ca^{2+} ion with respect to Ru^{4+} is responsible for the increased cell volume, as will be discussed in next section.

In order to exclude possible secondary phases formation, we performed specific investigations by SEM, EDX and XRD. SEM analyses never show presence of precipitates or segregations; the film surface is smooth and homogeneous at the scale of SEM resolution. EDX excludes stoichiometry inhomogeneities at the μm scale. No significant peak that could be attributed to secondary phases was ever found in XRD measurements. In particular, although some samples have a stoichiometry not far from that of 2:1:4, X-ray measurements did not reveal trace of reflections from the first element of the Ruddlesen-Popper series, Ca_2RuO_4 [12]. This is agreement with the expectation that the formation of such phase requires higher deposition temperature, as for Sr_2RuO_4 [13].

The Ca content strongly influences the transport properties. "A" films appear dark and shiny, with $\rho_{300} \approx 300-400$ $\mu\Omega$ cm. "B" samples show resistivity values spreading over an extremely wide range (up to 1 kΩ cm). With increasing resistivity, the color of samples changes from dark to yellowish and than to transparent.

We found that ρ_{300} is clearly related to volume of the $Ca_{1+x}Ru_{1-x}O_3$ cell. As reported in Figure 5, samples with a larger cell volume show higher resistivity values. The dotted line, which is reported just as a guide to the eye, suggests a grossly exponential dependence of resistivity on $\frac{V}{V_o}$ and therefore on the x value. Furthermore, while "A" samples show metallic behavior and resistivity values comparable to those normally reported for high quality CRO thin films, "B" samples show a completely different transport regime. It is shown that a crossover from a metallic to some thermally activated conduction regime takes place at some x value, which is intermediate between the typical ranges for "A" samples ($x < 0.06$) and "B" samples ($x > 0.19$). According to the amount of substitution, ρ_{300} may vary by over three orders of magnitude, and the resistivity at LHe ($\rho_{4,2}$) may vary by over six orders of magnitude.

3 Discussion

3.1 Structure and composition of CRO films

The previously reported data confirm that a solid solution with stoichiometry $Ca_{1+x}Ru_{1-x}O_y$, where Ca randomly substitutes Ru [5], can be grown in thin film form over a very wide range of the "x" variable. Let's now briefly discuss the possible substitution mechanisms. The linear behavior observed over the whole range of available data (Fig. 4) confirms that Vegard's law applies to our data and suggests a single mechanism of Ca/Ru substitution. In order to account for the charge neutrality, each substitution must also introduce 2 extra holes in the structure. Two plausible processes, leading to different electronic configurations, can be in principle envisaged:

a) oxygen vacancies are formed, leading to $Ca_{1+x}Ru_{1-x}O_{3-x}$ composition;
b) a Ru^{4+} is oxidized to a higher level, e.g., to Ru^{5+}.

We observe that the values of oxygen content as reported in Figure 1 do not support the hypothesis of oxygen depletion on substituted samples. Furthermore, the presence of Ru^{5+} has been previously reported in doped $CaRuO_3$ systems [14]. We tend therefore to believe that hypothesis b) is by far the most likely one.

By neglecting the volume change due to the shrinking of Ru ions as a consequence of the increased oxidation state, the volume increase should be directly attributed to the difference in size between Ca^{2+} (ionic radius $r_{Ca} = 114$ pm) and Ru^{4+} (ionic radius $r_{Ru} = 76$ pm). Different functional expression could be proposed, also according to the microscopic model of the cell deformation induced by substitution. Without discussing this aspect in detail, we will limit ourselves to observe that experimental behavior follows the Vegard's law, and can be reasonably described by the following very simple expression (dotted line in Fig. 4):

$$\frac{\Delta V}{V_o} = \frac{\left((2\, r_{Ca})^3 - (2\, r_{Ru})^3 \right)}{V_o} x. \qquad (1)$$

While a direct prove of the random Ca^{2+} substitution would require high resolution TEM, we stress that other plausible mechanisms are not supported by experimental data. For example, if the extra Ca were accommodated in excess Ca-O planes leading to microdefects with the Ruddelson-Popper structure, the lattice spacing would not be affected in contrast to data of Figure 4.

3.2 Growth kinetics and stoichiometry in CRO films

Our data show that Ca excess and lattice expansion are characteristic of "B" films, while "A" films always have a cell volume very close to the bulk CRO. Such direct relationship between orientation and stoichiometry has been repeatedly proven by comparing pairs of samples grown in the same deposition run. No direct relationship between unit cell size and substrate lattice parameters (as suggested in [5]) can instead be inferred. For example, in plane lattice parameters greater than those of bulk CRO (up to over 0.39 nm) are regularly found in samples deposited on $LaAlO_3$ ($a = 0.379$ nm) where compressive strain would be expected. Furthermore, the transport properties of the samples, as reported in Figure 6, show no correlation with the substrate lattice parameter, while the correlation with substrate orientation is striking.

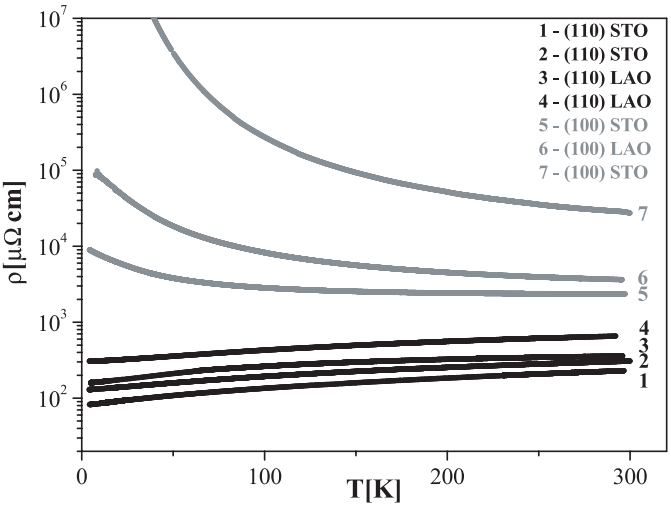

Fig. 6. $\rho(T)$ for CRO film grown on STO and LAO. Plots for "A" samples are black lines. Plots for "B" samples are gray lines.

The whole body of the reported experimental data demonstrate that different sticking coefficients C_s for the single atomic species are obtained on different growth surfaces. Hence, we recall some established aspects of the growth dynamics, with the aim of stressing the factors that can lead to an interpretation of our results. It is known that volatile oxides are present in the Ru phase diagram, in oxidizing conditions, while the same does not apply to Ca. During film growth, Ru atoms adsorbed on the film surface (adatoms) can go through two competing processes. Part of them are captured by the growing front of the CRO thin film, with the characteristic time τ_c . More precisely, this process is determined by chemisorption at specific sites, such as vacancies, step edges and kinks on the film surface. However, Ru adatoms may as well be oxidized to the highest level, and leave the substrate in the form of a volatile oxide (e.g. RuO_3, RuO_4) [15], with a characteristic time τ_a. The formation of vapors of highly oxidized Ru has been acknowledged by several authors [16] as the mechanism driving Ru desorption in RuO_2 thin films. We stress that the desorption of the weakly bonded adatoms is easier than Ru desorption from bulk (a process that actually takes place over 800 °C) [15].

The growth is characterized by sticking coefficients $C_s < 1$ when a desorption process is effective, i.e. when τ_a becomes at least comparable to τ_c. These characteristic times are affected by several parameters, including substrate temperature and growth rate [1]. In our case, the rate of Ru desorption as RuO_x may also be increased by the abundance of oxygen and possibly by some backsputtering (due to the on-axis sputtering configuration). We

believe that, due to the exponential dependence of τ_a on T, Ru volatility could also explain the dependence of transport properties on substrate temperature reported in [7].

The key point is whether Ru volatility can or cannot depend on crystallographic orientation of the substrate. Although several speculations on the different growth modes of a $(110)_{\text{p.c.}}$ and $(100)_{\text{p.c.}}$ perovskite surface could be proposed, we will only point out a few differences between the two cases.

a) The number and location of stable sites for adatoms may depend on the crystallographic orientation. In fact, in epitaxial films growth, the orientation of the substrate is continued into the film structure. Then the nature of the film surface exposed to vapor during deposition is connected to substrate orientation, because terminating surfaces of films with different crystallographic orientation are different.
   A wide literature proves that during $(100)_{\text{p.c.}}$ growth, $(100)_{\text{p.c.}}$ terraces terminate the films of simple perovskites. The case of $SrRuO_3$ has been investigated in [17]; we believe that the same is true for CRO. In that case, there are two possible (100) terminations, corresponding to the Ca-O plane or instead to the Ru-O plane. Unless special deposition processes are set, both terminations may appear at the same time, each one forming (100) terraces. If this is the case, each $(100)_{\text{p.c.}}$ terrace would contain available sites for one cation type, because Ca-O and Ru-O_2 planes are stacked over each other.
   Less is known about the growth of (110) oriented films. Studies of surface reconstruction of simple perovskites [18] have demonstrated the stability of (110) facets, but under specific conditions have also shown that (100)/(010) faceting at the microscopic level is also possible. These results suggest that the actual terminating layers during growth may as well be (110) terraces, or alternatively rough surfaces characterized by some faceting. In any case, the terminating layer is expected to contain a high density of both Ca and Ru sites.
b) The adatom binding energy depend on the crystallographic orientation of the terrace surface, because of the different number of nearest neighbors. A Ru adatom would have one nearest O neighbor on an ideal $(100)_{\text{p.c.}}$ terrace, while it would have two nearest O neighbors on a $(110)_{\text{p.c.}}$ terrace, and perhaps even more when roughness providing microscopic facets, ledges and kinks is accounted for.

All these circumstances point to a faster capture of adatoms on $(110)_{\text{p.c.}}$ surfaces. As an example, a Ru adatom adsorbed on a RuO terrace of a $(100)_{\text{p.c.}}$ CRO film must reach a terrace ledge within its diffusion length to find a stable site in the lattice. On the other hand, a Ru adatom adsorbed on a terrace of a $(110)_{\text{p.c.}}$ CRO film finds available sites within a lattice spacing. On this basis, we argue that Ru desorption only becomes competitive with Ru capture when (100) perovskite substrates are employed, thus yielding Ru deficient films. On the contrary, we believe that Ru desorption is negligible for $(110)_{\text{p.c.}}$ CRO films, as obtained on (110) STO, LAO and $(110)_{\text{p.c.}}$ NGO.

It is worthwhile to stress that the case of ruthenates is quite peculiar in respect to other simple perovskites, such as titanates, manganites, etc. Difference in stoichiometry of films grown on (100) or (110) substrates was never observed, to our knowledge, in such systems. In the framework of the foregoing considerations, the explanation relies upon the existence of volatile Ru oxides, that have no correspondence in the other mentioned cases.

As a final consideration, we notice that a high volatility of Ru makes growth conditions less stable. We argue that this explains the noticeable differences in the properties among "B" samples (see, e.g., data reported in Figs. 4, 5). On the contrary, a very high reproducibility is achieved in the case of "A" samples.

3.3 The $Ca_{1+x}Ru_{1-x}O_3$ phase and its transport properties

Summarizing the previously reported data, there is strong experimental evidence that our samples are single phase. This implies that excess Ca does not segregate in precipitates, but is included in a Ca rich solid solution. This statement is supported not only by the absence of any trace of precipitates in XRD patterns and SEM images, but it is confirmed by the regular dependence of cell volume (Fig. 4, Eq. (1)), room temperature resistivity (Fig. 5) and resistivity ratio $\frac{\rho_{300}}{\rho_{4,2}}$ (Fig. 6) as a function of x. It is in fact hard to believe that conglomerates dispersed in the body of the film can lead to the reported resistivity variations. This would require attainment of a percolative regime, in which electrical transport takes place though channels connecting separate conductive regions. However, in the percolative regime, a power-law dependence of resistivity vs. impurity content is expected, that is not found in our case. A crossover from two different conduction regimes as described in Figure 6 could also not be explained in such a framework.

We can therefore conclude that a Ca rich phase spanning a wide stoichiometry range, and not reported before to our knowledge, is found in our samples. We speculate that this might be a metastable phase, that would at higher temperatures separate in a mixture of $CaRuO_3$ and Ca_2RuO_4. The physical origin of the metal-insulator transition that takes place at increasing x, and of the peculiar $\rho_{300}(x)$ dependence reported in Figure 5, are interesting open questions that are beyond the scope of this paper.

4 Conclusions

We have deposited calcium ruthenate films on various different perovskitic substrates. The growth orientation is always "cube on cube", so that $(110)_{\text{p.c.}}$ orientation (type "A" samples) is obtained on (110) STO and LAO, and $(100)_{\text{p.c.}}$ NGO, while $(100)_{\text{p.c.}}$ orientation (type "B") is achieved on (100) STO and LAO, and $(110)_{\text{p.c.}}$ NGO.

An important result emerging from our work is that several physical and chemical properties of sputtered calcium ruthenate films, and in particular stoichiometry, can depend dramatically on growth orientation. When several different substrates are employed during the same deposition run, "A" samples are high quality, stoichiometric, metallic and strained [4], while "B" samples are not matched to the substrate, present noticeable deviations from the 1:1:3 stoichiometry, and poor conduction quality.

We studied the details of the structure of "B" samples, demonstrating that they are free of spurious phases. Our data support the idea that the extra Ca ions randomly substitute Ru, even for the largest Ca excess. Films of a single-phase solid solution, with Ca/Ru ratio varying in a wide range, are therefore obtained by our sputtering technique. The typical orthorhombic distortion of $CaRuO_3$ is preserved in Ca-rich films at moderate Ca excess. The distortion is reduced with increasing Ca content, and the samples approach a tetragonal structure. This is probably a cubic phase deformed by strain due to substrate.

The deviations from the correct stoichiometry, cell volume and transport regime in our samples cannot be attributed to stress. For instance, in plane lattice parameters greater than those of bulk CRO (up to over 0.39 nm) are regularly found in samples deposited on (100) $LaAlO_3$ ($a = 0.379$ nm) where compressive strain would be expected. In general, we obtained quite similar properties on samples deposited on LAO and STO, possessing lattice parameters respectively smaller and bigger than the CRO pseudocubic cell. We suggest an interpretation of the reported differences between the A and B samples in terms of different growth mechanisms. The relevant parameters in our approach are the characteristic times for Ru capture and Ru desorption as a volatile oxide. Qualitative considerations suggest that these characteristic times depend on the crystallographic orientation of the terraces at the growing film surface, and that desorption may be enhanced in the case of (100) planes.

Finally, our results confirm the dramatic variability of transport properties of CRO with doping. The availability of samples with different Ca content allows spanning the entire phase diagram ranging from an insulator to a non-conventional metal.

References

1. See, e.g., A. Pampinelli, J. Villain, *Physics of Crystal Growth* (Cambridge University press, 1998)
2. G. Cao, S. Mc Call, M. Shepard, J.E. Crow, R.P. Guertin, Phys. Rev. B **56**, 321 (1997)
3. I. Felner, I. Nowik, I. Bradaric, M. Gospodinov, Phys. Rev. B **62**, 11332 (2000)
4. F. Ricci, M.F. Bevilacqua, F. Miletto Granozio, U. Scotti di Uccio, Phys. Rev. B **65**, 155428 (2002)
5. R.A. Rao, Q. Gan, C.B. Eom, R.J. Cava, Y. Suzuki, J.J. Krajewski, S.C. Gausepohl, M. Lee, Appl. Phys. Lett. **70**, 3035 (1997)
6. J.S. Ahn, J. Bak, H.S. Choi, T.W. Noh, J.E. Han, Yunkyu Bang, J.H. Cho, Q.X. Jia, Phys. Rev. Lett. **82**, 5321 (1999)
7. S. Hyun, J.H. Cho, A. Kim, J. Kim, T. Kim, K. Char, Appl. Phys. Lett. **80**, 1574 (2002)
8. G. Cao, F. Freibert, J.E. Crow, J. Appl. Phys. **81**, 3884, (1997)
9. L. Capogna, A.P. Mackenzie, R.S. Perry, S.A. Grigera, L.M. Galvin, P. Raychaudhuri, A.J. Schofield, C.S. Alexander, G. Cao, S.R. Julian, Y. Maeno, Phys. Rev. Lett. **88**, 76602 (2002)
10. F. Miletto Granozio, F. Ricci, U. Scotti di Uccio, J.C. Villegier, Phys. Rev. B **57**, 6173 (1998)
11. G. Malandrino, G. Condorelli, I. Fragalà, F. Miletto, U. Scotti di Uccio, M. Valentino, Physica C **271**, 83 (1996)
12. M. Braden, G. André, S. Nakatsuji, Y. Maeno, Phys. Rev. B **58**, 837 (1998); S. Nakatsuji, S. Ikeda, Y. Maeno, J. Phys. Soc. Jpn **66**, 1868 (1997)
13. Mark A. Zurbuchen, Yunfa Jia, Stacy Knapp, Altaf H. Carim, Darrell G. Schlom, Ling-Nian Zou, Ying Liu, Appl. Phys. Lett. **78**, 2351 (2001)
14. I.M. Bradaric', I. Felner, M. Gospodinov, Phys. Rev. B **65**, 024421 (2001); I. Felner, U. Asaf, I. Nowik, I. Bradaric, Phys. Rev. **66**, 054418 (2002)
15. W.E. Bell, M. Tagami, J. Phys. Chem. **67**, 2432 (1963)
16. Jeong-gun Lee, Young Tae Kim, Suk-ki Min, Sung Ho Choh, J. Appl. Phys. **77,** 5473 (1995)
17. R.A. Rao, Q. Gan, C.B. Eom, Appl. Phys. Lett. **71**, 1171 (1997)
18. See e.g., K. Szot, W. Speier, Phys. Rev. B **60**, 5909 (1999)